Academic Journal of Science and Technology
ISSN: 2771-3032 | Vol. 10, No. 2, 2024

Quantitative Inversion of Soil Salinity in Different Seasons in Huinong District, Ningxia based on Sentinel-2 satellite

Tuo Wang, Xiaojing Shen*, Wenjie Luan

School of Civil and Water Resources Engineering, Ningxia University, Yinchuan 750021, Ningxia, China
* Corresponding author

Abstract: Salinisation of agricultural soils poses an important constraint to sustainable agricultural development, especially in the Huinong region of Ningxia, northwestern China, where salinised soils are widely distributed. However, due to the limitations of monitoring technology, the detailed situation of soil salinisation in this region is not known. Currently, the multispectral instrument (MSI) on board the Sentinel-2 satellite provides a good opportunity for monitoring soil salinity dynamics. Therefore, in this study, the feasibility of using the multispectral instrument (MSI) on board the Sentinel-2 satellite, combined with a machine learning model, to accurately monitor the soil salinity content during the spring and summer seasons was explored. And three additional red-edge bands (B5-B7) were used instead of the traditional red band (B4) to generate potential soil salinity indices. A screening method based on the PLS-VIP criterion was used to screen the spectral covariates, and three machine learning methods, namely, Random Forest (RF), Support Vector Machine (SVM) and Extreme Learning Machine (ELM), were employed to build the inverse model of soil salt content. The results showed that the Random Forest model based on Sentinel-2 imagery performed the best in the inversion with good prediction results, with R2 and RE of 0.825 and 0.207 and 0.711 and 0.271 in spring and summer, respectively.The study also revealed that soil salinity varied significantly between seasons, and was higher in spring than in summer. This result is of great significance as a guide for soil salinity monitoring and land reclamation in arid or semi-arid regions.

Keywords: Satellite remote sensing, variable screening, inversion modelling, spectral indices; machine learning.

1. Introduction

Soil salinisation is a global problem that seriously affects soil resources and ecosystems. More than 1 billion hectares of land in hundreds of countries and regions around the world are threatened by salinity problems. High levels of soil salts are detrimental to crop growth, directly affecting crop yields and threatening land quality and sustainable development and use, as well as sustainable agriculture[1]. Accumulation of salt leads to soil degradation, especially in arid and semi-arid areas. Due to environmental, social and economic backwardness, in arid and semi-arid areas, salts migrate from deeper soil layers and accumulate in topsoil with evaporative water intensive irrigated agricultural production. Rational use of salinity-affected lands can increase the area of arable land and reduce the pressure between agricultural production and urban development. Effective management of salinity-affected soils requires accurate and efficient monitoring and mapping of soil salinisation. Various methods and platforms are being used to quantify the salt content of different soil depth intervals. Soil electrical conductivity (EC) is often used for dynamic monitoring of soil salinity due to its strong correlation with soil salinity[2]. Traditional methods of soil conductivity analysis, which mainly involve on-site sampling and bringing soil samples back to the laboratory for processing, have high accuracy, but are unable to monitor soil salinity on a large scale and make multiple measurements. As an alternative, satellite remote sensing (RS) technology can provide a large amount of information about the soil, and the satellite remote sensing method has the advantages of wide spatial coverage and high resolution compared with traditional field measurements.

Saline soils typically exhibit higher albedo compared to non-saline soils and salt accumulation on the soil surface can be theoretically observed using remote sensing imagery. Optical remote sensing satellites can directly record the spectral reflectance of soil salinisation.The Sentinel-2 satellite equipped with a Multispectral Instrument (MSI) launched in 2015 provides 13 spectral bands ranging from 443 nm to 2,190 nm. The provided spectral images have high spatial resolution, multispectral bands and short revisit time, which makes them advantageous for soil monitoring.Gorji et al[3] detected soil salinity changes (0.0-0.2 m) at the field scale using Sentinel-2 satellite. At the regional scale, Wang et al[4] used Sentinel-2 multispectral scanning imaging (MSI) satellite to estimate surface soil salinity (0.0-0.2 m) in the Lake Ebinur region.Bannari et al [5] applied VIS-NIR and SWIR spectral bands of Sentinel 2-MSI for soil salinity detection in the Kingdom of Bahrain and showed that the data's potential in soil salinity discrimination. Based on remote sensing imagery, researchers have developed various vegetation, salinity and soil indices to estimate soil salinity [6]. In addition, many modelling approaches such as partial least squares regression, random forest, support vector machine regression, artificial neural networks and convolutional neural networks have been widely used to predict soil salinity changes. In order to improve the model performance, methods such as Pearson correlation analysis, grey correlation analysis, genetic algorithms, and random forests have been used to select the best covariates to be used in the final model. However, the contribution of different remote sensing indices (or covariates) to the salt estimation model is site-specific as they are affected by land cover type and other surface parameters.

Therefore, in this study, the feasibility of using the Multispectral Instrument (MSI) on board the Sentinel-2 satellite in conjunction with a machine learning model to accurately monitor soil salinity content during the spring and summer seasons was explored. And three additional red-edge bands (B5-B7) were used instead of the traditional red band (B4) to generate potential soil salinity indices. A screening method based on the PLS-VIP criterion was used to screen the spectral covariates, and three machine learning methods, namely, Random Forest (RF), Support Vector Machine (SVM) and Extreme Learning Machine (ELM), were employed to build the inverse model of soil salt content.

2. Materials and Methods

2.1. Overview of the study area

The study area is located in Huinong District, Shizuishan City, Ningxia Hui Autonomous Region. Its geographical coordinates are between 38°05' and 38°38' north latitude and 105°07' and 106°09' east longitude. The area is relatively flat and is one of the important agricultural production areas in Ningxia. It is a typical inland arid climate zone with large temperature differences between seasons. The average annual precipitation is 292 mm; the average annual evaporation is 2,444 mm, mainly in summer and autumn. Crop cultivation is dominated by maize, and it is one of the regions in China with a high concentration of saline and alkaline land, with relatively serious problems of soil salinisation.

2.2. Experimental data collection and pre-processing

2.2.1. Collection and determination of soil samples

A combination of soil type, soil surface characteristics, and prior field sampling experience were considered. A total of 86 soil samples were collected on 28 May 2023 and 24 July 2023, including 43 soil samples in spring and 43 samples in summer. Sampling depths ranged from 0-20 cm, and latitude and longitude coordinates of sampling sites were recorded. The collected soil samples were placed sequentially in aluminium boxes according to the assigned numbers and subsequently brought back to the laboratory for experimental analysis. The moisture content of the soil was determined by oven drying method. The procedure for the determination of soil electrical conductivity (EC, us/cm) consisted of grinding the dried soil samples and preparing them into a 1:5 (soil to water ratio) solution. Subsequently, conductivity values were determined using a conductivity meter (Model MTD 15) after routine operations such as stirring, standing, settling and filtration. The formula for calculating soil salinity (SSC, %) entailed calibrating the relationship between soil conductivity and soil salinity by conducting a large number of soil conductivity and drying salinity correspondence tests as.

$$Y = 0.0054951 \times X - 0.00131 (R^2 = 0.998) \quad (1)$$

Where: Y is the salt content of the soil, g/kg; X : the electrical conductivity of the soil, μs/cm.

2.2.2. Acquisition and processing of Sentinel-2 satellite images

Soil salinity in the study area was estimated using Sentinel-2 time-series satellite data, Sentinel-2 satellite images were downloaded from the ESA Copernicus Data Centre (Open Access Hub (copernicus.eu)), and the sampling time of the field experiments coincided with the time of Sentinel-2 satellite image collection. The time span of the study was from May 2023 to July 2023. Using ENVI 5.6.3 software, image preprocessing was performed through radiometric calibration, geometric correction, and atmospheric correction steps, and reflectance data were acquired at the sampling sites.

2.3. Construction of spectral indices

Based on the soil salinity index listed in Table 1 as the reference spectral salinity index and incorporating the new spectral functions of the three additional red-edge bands (B5-B7)[7], this study substitutes these three bands (B5-B7) for B4 and calculates the various possible combinations of these new red-edge bands to generate the potential soil salinity indices for the estimation of conductivity (Table 2).

Table 1. Reference spectral salinity index

salinity index	equation	salinity index	equation
Int1	$(B3 + B4) / 2$	S1	$B2 / B4$
Int2	$(B3 + B4 + B8a)$	S2	$(B3 - B4) / (B3 + B4)$
SI	$\sqrt{B3 \times B4}$	S3	$(B3 \times B4) / B2$
SI1	$\sqrt{B3 \times B4}$	SI-T	$B4/B8a \times 100$
SI2	$\sqrt{(B3)^2 + (B4)^2 + (B8a)^2}$	NDSI	$\sqrt{(B3)^2 + (B4)^2}$
SI3	$\sqrt{(B3)^2 + (B4)^2}$		

Table 2. Newly proposed red-edge spectral indices

salinity index	equation	salinity index	equation
Int1 re1	$(B3 + B5) / 2$	S3 re3	$(B3 \times B7) / B2$
Int1 re2	$(B3 + B6) / 2$	SI-T re1	$B5 / B8a \times 100$
Int1 re3	$(B3 + B7) / 2$	SI-T re2	$B6 / B8a \times 100$
Int2 re1	$(B3 + B5 + B8a)$	SI-T re3	$B7 / B8a \times 100$
Int2 re2	$(B3 + B6 + B8a)$	SI re1	$\sqrt{B2 + B5}$
Int2 re3	$(B3 + B7 + B8a)$	SI re2	$\sqrt{B2 + B6}$
NDSI re1	$(B5 - B8a) / (B5 + B8a)$	SI re3	$\sqrt{B2 + B7}$
NDSI re2	$(B6 - B8a) / (B6 + B9a)$	SI1 re1	$\sqrt{B3 \times B5}$
NDSI re3	$(B7 - B8a) / (B7 + B10a)$	SI1 re2	$\sqrt{B3 \times B6}$
S1 re1	$B2 / B5$	SI1 re3	$\sqrt{B3 \times B7}$
S1 re2	$B2 / B6$	SI2 re1	$\sqrt{(B3^2 + B5^2 + B8a^2)}$
S1 re3	$B2 / B7$	SI2 re2	$\sqrt{(B3^2 + B6^2 + B8a^2)}$
S2 re1	$(B3 - B5) / (B3 + B5)$	SI2 re3	$\sqrt{(B3)^2 + (B7)^2 + (B8a)^2}$
S2 re2	$(B3 - B6) / (B3 + B6)$	SI3 re1	$\sqrt{(B5)^2 + (B3)^2}$
S2 re3	$(B3 - B7) / (B3 + B7)$	SI3 re2	$\sqrt{(B6)^2 + (B3)^2}$
S3 re1	$(B3 \times B5) / B2$	SI3 re3	$\sqrt{(B7)^2 + (B3)^2}$
S3 re2	$(B3 \times B6) / B2$		

2.4. Screening of spectral indices

Considering that too many spectral indices may lead to redundant information, the study chose the partial least squares-based variable projection importance (PLS-VIP) criterion for independent variable screening[8]. With this criterion, they constructed the spectral indices as a combination of variables in spring and summer seasons as input independent variables for the soil salinity inversion model. In the spring and summer seasons, the study considered the variables greater than 1 as significant to the measured soil salinity based on the PLS-VIP calculation results and used them as the independent variables of the satellite remote sensing inversion model.

The principle of PLS-VIP criterion is given in the following equation.

$$VIP_j = \sqrt{\frac{p\sum_{h=1}^{m} R(Y,t_h)w_{hj}^2}{\sum_{h=1}^{m} R(Y,t_h)}} \quad (2)$$

where p is the number of independent variables; m is the number of components extracted from the original variable species by partial least squares (PLS); t_h is the hth component; $R(Y,t_h)$ is the explanatory power of component t_h on the dependent variable Y, which is usually the square of the correlation coefficient of the two; W_p is the jth component of the axis w_h and W_p is the eigenvector of the matrix ${X_{h-1}}^T, Y_{h-1}Y_{h-1}^T, X_{h-1}$ eigenvectors.

When the PLS-VIP value of an independent variable is greater than 1, it means that the independent variable has an important role in explaining the dependent variable Y, while when the PLS-VIP value is less than 1, it means that the independent variable has a less important role[9].

2.5. Construction of soil salinity inversion model

2.5.1. Random Forest Method (RF)

Random Forest Model (RF) is an integrated method based on decision trees with excellent generalisation performance, which can be widely applied to regression and classification problems[10]. The prediction error is estimated by generating classification and regression trees using the bagging algorithm, using the randomly selected training set as an independent dataset and the unselected data as out-of-bag data. At the nodes of each decision tree, the covariates are also randomly divided into multiple groups to minimise the variance of the split groups, thus completing the tree splitting process. The performance of random forests is usually evaluated by out-of-bag error (errOOBt), while Variable Importance (VI) is based on accuracy, using the significance of mean square error (% IncMSE) and node purity (IncNodePurity) to rank them. For each tree (t) in the random forest, the RF Variable Importance of Xi can be calculated as in equation (3) below.

$$VI(X^i) = \frac{1}{ntree}\sum_t \left(err\tilde{OO}_t^i - errOOB_t\right) \quad (3)$$

where t denotes each tree in the forest; OOBt denotes the relevant part of the bootstrap process used to construct t that is not included; errOOBt is the error of a specific tree t on the relevant OOBt sample; $err\tilde{OO}_t^i$ denotes the perturbed samples affected by the values of Xi alignment. In this study, the size of the subset of input variables was set to 23 by repeated tests, and the number of trees was set to 500 based on the stability properties of $err\tilde{OO}_t^i$.

2.5.2. Extreme Learning Machines (ELM)

ELM is a relatively new computational (or data intelligence) model designed to address the shortcomings of classical machine learning models.The computation in ELM does not require iterations as in gradient-based algorithms. In addition, the hidden nodes of ELM can be randomly generated and the output weights can be solved by least squares.ELM has the advantages of convenience, high learning efficiency, and greater adaptability to some nonlinear activations and kernel functions.

2.5.3. Support Vector Machines (SVM)

Support Vector Machine (SVM) is a supervised machine learning technique with intelligent design. It was originally proposed by Boser, Guyon and Vapnik in 1992[11].SVMs use learning algorithms based on statistical learning theory and optimisation theory to enable computer programs to learn how to achieve classification and regression tasks, improve prediction accuracy and avoid overfitting.The basic idea of SVMs is to use the Vapnik- based Chervonenkis (VC) dimension-based structural risk minimisation (SRM) principle to find hyperplanes and separate data in high-dimensional spaces. Compared to complex neural network functions, SVMs are popular for their high empirical performance while avoiding local minima.

2.6. Evaluation indicators

In order to evaluate and compare the overall performance of the estimation models, the study introduced the coefficient of determination (R^2) and the relative error (RE) to comprehensively assess the fitting effect, in which the closer the R^2 is to 1 and the smaller the RE is, the higher the accuracy of the inversion model of soil salt content is.

$$R^2 = \frac{\sum_{i=1}^{n}(\hat{y}_i - \overline{y})^2}{\sum_{i=1}^{n}(y_i - \overline{y})^2} \quad (4)$$

$$RE = \frac{1}{n}\sum_{i=1}^{n}\left|\frac{\hat{y}_i - y_i}{y_i}\right| \quad (5)$$

where n is the number of soil samples; $\hat{y}_i$ is the predicted value; $\bar{y}$ is the mean value; and y_i is the measured value.

3. Results and Analyses

3.1. Statistical results of measured soil salinity data in the study area

To ensure generalisation and robustness of the model, all soil samples (collected in spring and summer) were considered as one dataset in this study. The dataset contains a total of 86 samples and is divided into two parts using Kennard-Stone (K-S)[12]: 55 soil samples constitute the calibration set and 31 soil samples constitute the validation set as shown in Table 3. The two sets were used for cross-validation and independent validation, respectively.

Table 3. Division of training and validation sets

Depth/cm	Data sets	Type of sampling point				Salinity (g/100g)	
		unsalted (<0.2%)	mild salinisation (0.2%~0.5%)	Heavy salinisation (0.5%~1.0%)	salted soil (>1.0%)	SD%	CV
0-20	Total Sample	24	39	21	2	2.85	0.62
	Training Set	15	24	15	1	2.94	0.62
	Validation Set	9	15	6	1	3.02	0.61

The mean value of soil salinity in the study area was 4.855 g/kg in spring (May) and 2.548 g/kg in summer (July) (Fig. 1). According to the soil salinity grading criteria [10], most of the study area is in the region of moderate to light salinity, but there are some areas with heavy salinity. This situation is basically consistent with the growth of crops in the study area.

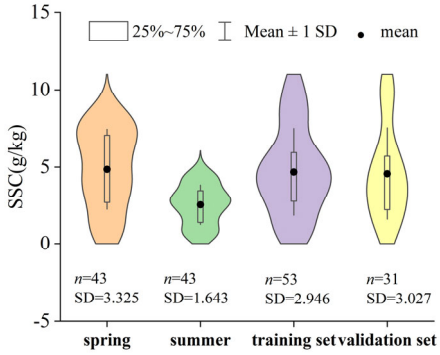

Figure 1. Soil descriptive statistics

3.2. Comparison of the red edge index with existing soil salinity indices

A comparison was made between existing soil salinity indices and soil salinity data extracted from the Huinong district. Considering the new spectral capabilities of the three additional red-edge bands, three bands (B5-B7) were used in this study instead of B4, and all of the published indices showed significant correlations with conductivity at the 0.01 level ($p < 0.01$), except for the NDSI, S1, and S2, which were relatively unsatisfactory. These three indices will be discussed separately in this study. An increase in correlation can be observed when replacing the red band with the red-edge band (Fig. 2). The introduction of the red-edge band enhanced the sensitivity of the salinity index to soil salinity, probably because of the novel spectral information and higher signal-to-noise ratio in the red-edge region. For the three less desirable ones (NDSI, S1 and S2), the improvement with the introduction of the red-edge bands was not satisfactory. However, these less predictive spectral covariates were not excluded from this study.

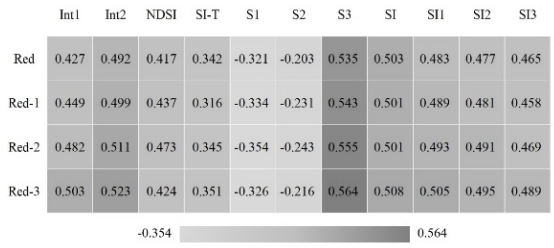

Figure 2. Correlation between electrical conductivity and different soil salinity indices (existing and derived red-edge indices)

3.3. Spectral index combinations based on correlation analysis

The study used a screening method based on the PLS-VIP criterion for 44 spectral covariates (11 existing soil salinity indices, 33 red-edge indices). Variables with results greater than 1 calculated by PLS-VIP were considered as more important variables for the measured soil salinity and were used as independent variables in the satellite remote sensing inversion model.The results of the PLS-VIP criterion screening are shown in Fig. 3, and a total of 11 variables were screened (Int2, SI2, S2, Int1re1, NDSI re1, S2 re2, S3 re3, SI re2, SI1 re1, SI2 re2, SI3 re1). Compared with the initial 44 variables provided, the screening method based on the PLS-VIP criterion greatly reduces the number of variables, which effectively reduces the amount of model calculations and saves time for the study to construct the model. It can also be seen that the calculation results of the newly proposed red-edge spectral index are overall greater than the existing soil salinity index, thanks to the fact that this additional spectral information can provide more spectral information for analysis and identification. At the same time, the B4 band may be affected by atmospheric influences, resulting in masked or distorted signals. The use of the B5-B7 bands may reduce atmospheric effects.

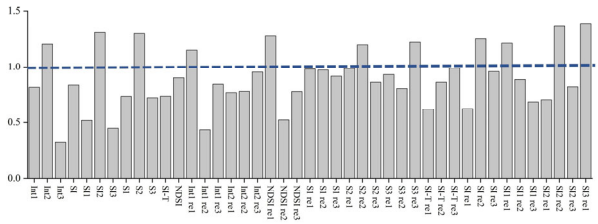

Figure 3. PLS-VIP calculation result

3.4. Establishment and comparison of soil salinity inversion models

The combination of spectral variables determined by the screening method based on the PLS-VIP criterion was used as the input independent variables, and the corresponding inversion models were established for the measured soil salinity values in spring and summer seasons using three modelling methods, namely RF, SVM and ELM. These inverse models were comprehensively evaluated and statistically analysed by comparing the predicted values of the validation set with the actual soil salinity, and the results are displayed in Fig.4. From the figure, it can be seen that most of the models have good stability when it comes to the processed soil inversion models, and their coefficients of determination, R^2, are within a reasonable range From the perspective of the three depths, among the inversion models of soil salinity established by spectral covariates screened by the screening method based on the PLS-VIP criterion, the RF model has the highest inversion accuracy, followed by the

SVM model, while the ELM model performs the worst. In addition, the accuracy of these models was significantly higher in spring than in summer. The possible reason for this is that there is mainly vegetation cover in summer, which causes a decrease in the accuracy of the models. Comparing the three inversion models together, it can be concluded that the Random Forest model screened based on the PLS-VIP criterion shows better results both in spring and in summer.

Therefore, for the Sentinel-2 satellite remote sensing images during the whole spring and summer seasons, the screening method based on the PLS-VIP criterion was used to determine the combination of spectral variables in the spring and summer seasons and to establish the RF-based inversion model for soil salinity. The inversion effect is shown in Fig. 5. As can be seen from Fig. 5, within the four months, the RF-based model has a deep inversion accuracy, the R^2 of the validation set is between 0.641 and 0.825, with a better fitting ability, and the RE is between 0.197 and 0.319, with a smaller model error, and the inversion accuracy of the model is high.

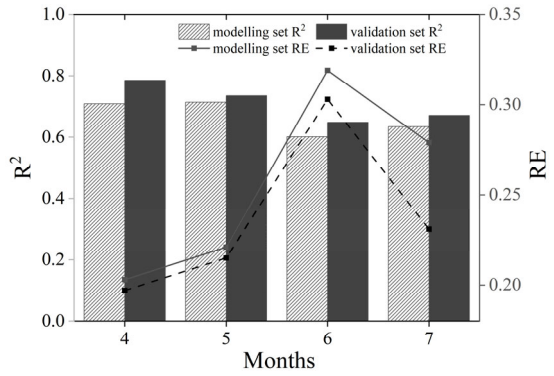

Figure 5. Predictive performance of the model

In the study, variables with results greater than 1 obtained through PLS-VIP calculations were considered as variables important to the measured soil salinity and were used as independent variables in the satellite remote sensing inversion model. Sampling Random Forest (RF) for model building and inversion of soil salinity using the trained model, soil salinity values were calculated for each image element in the study area and spatial distribution map of soil salinity was generated as shown in Fig. 6. The mean value of soil salinity was found to be 4.855 g/kg in spring and 2.548 g/kg in summer.Most of the study area is moderately salinised land and a small portion of heavily salinised land. This is in general agreement with the findings of Jia Zhuangzhuang[14] in 2023. The main causes of salinisation in this area are as follows:

Firstly, the topographic conditions make it downstream of the irrigation area, while pooling drainage and salt removal from upstream, and the relatively low-lying areas of the Helan Mountain hilly land and areas along the Yellow River, where the water flow pooling and drainage are obstructed, leading to the formation of moderately and heavily saline land. Secondly, soil characteristics are also a key factor. The soils around Yanzidun Township and Lihe Township are sticky and heavy, with poor infiltration properties, and the lateral flow of groundwater is difficult, resulting in the formation of partially alkaline soils. In addition, soil salinity in Huinong District ranges from 1.78 to 5.60 g/kg[15], with mildly saline soils occupying 62% of the total saline area. Secondly, the groundwater table is shallow and affected by the top support of the Yellow River water, with high mineralisation and widespread salt return. Yellow River water breaks or excessive upstream water consumption leads to insufficient downstream irrigation water, which affects the salt discharge from the arable land and also creates poor drainage problems.

4. Conclusion

In this study, the fitted relationships between bands and salinity indices and soil salinity were explored using field sampling data and Sentinel-2 data. Considering the new spectral functions of three additional red-edge bands, three bands (B5-B7) were used instead of B4, and various possible combinations of these new red-edge bands were calculated to generate potential soil salinity indices for estimating conductivity. The quantitative inversion of soil salinity and model accuracy validation were also carried out in Yinbei Huinong District, Ningxia. The combinations of spectral variables identified by the screening method based on the PLS-VIP criterion were used as input independent variables, and three machine learning methods, namely, Random Forest (RF), Support Vector Machine (SVM), and Extreme Learning Machine (EML), were introduced for modelling. The combination of sensitive spectral variables in spring and summer seasons was constructed, and the inverse model of soil salt content was established. Finally, the distribution of soil salt content in spring and summer seasons in the study area was mapped based on the optimal model. The results showed that among the soil salt content inversion models established based on the spectral bands and spectral indices of Sentinel-2 imagery, the model established by using Random Forest (RF) had the best accuracy and good prediction effect. This indicates that the Sentinel-2 data can reliably predict the distribution of soil salinity, while the machine learning model is able to deal with the nonlinear relationship between spectral information and soil salt content and reduce the covariance between variables, thus greatly improving the accuracy and efficiency of prediction. These findings provide a reliable reference for land use planning and management.

The size of spatial resolution and different scales will have an impact on the fitting results. This study was conducted only at the same scale, but considering the variability of geographic environments, multiple scales should be tried in future studies to better understand the correlation between spectral variables and soil salinity in this region. In addition, the failure to overcome the poor correlation between soil salt content and spectral reflectance under vegetation cover conditions resulted in the poor accuracy of the summer inversion model constructed on the basis of these images in monitoring the soil salt content, which is difficult to accurately reflect the actual spatial pattern. In order to improve the accuracy, a decision tree of salt depth with the normalised vegetation index (NDVI) as the branching criterion can be constructed to determine the optimal depth for soil salt content inversion. Subsequently, a category decision tree with NDVI and surface soil water content as branching criteria can be constructed to divide the soil samples into different categories, so as to establish soil salt inversion models separately.

References

[1] Metternicht G I, Zinck J A. Remote sensing of soil salinity: potentials and constraints[J]. Remote sensing of Environment, 2003, 85(1): 1-20.

[2] Zhitao Z , Guangfei W , Zhihua Y ,et al.Soil Salt Inversion Model Based on UAV Multispectral Remote Sensing[J].Transactions of the Chinese Society for Agricultural Machinery, 2019.

[3] Gorji T, Yildirim A, Hamzehpour N, et al. Soil salinity analysis of Urmia Lake Basin using Landsat-8 OLI and Sentinel-2A based spectral indices and electrical conductivity measurements[J]. Ecological Indicators, 2020, 112: 106173.

[4] Wang Y, Deng C, Liu Y, et al. Identifying change in spatial accumulation of soil salinity in an inland river watershed, China[J]. Science of the Total Environment, 2018, 621（15）: 177-185.

[5] Bannari A, El-Battay A, Bannari R, et al. Sentinel-MSI VNIR and SWIR bands sensitivity analysis for soil salinity discrimination in an arid landscape[J]. Remote Sensing, 2018, 10(6): 855.

[6] Hoa P V, Giang N V, Binh N A, et al. Soil salinity map** using SAR sentinel-1 data and advanced machine learning algorithms: A case study at Ben Tre Province of the Mekong River Delta (Vietnam)[J]. Remote Sensing, 2019, 11(2): 128.

[7] Hong Y, Liu Y, Chen Y, et al. Application of fractional-order derivative in the quantitative estimation of soil organic matter content through visible and near-infrared spectroscopy[J]. Geoderma, 2019, 337: 758-769.

[8] Wang M, Wang J, Chen J, et al. Effect of commercial yeast starter cultures on Cabernet Sauvignon wine aroma compounds and microbiota[J]. Foods, 2022, 11(12): 1725.

[9] Tao Z, Cun-Yong J U, Ti-jiu C A I, et al. Selection of parameters for estimating canopy closure density using variable importance of projection criterion[J]. Journal of Beijing Forestry University, 2010, 32(6): 37-41.

[10] Jia P, Shang T, Zhang J, et al. Inversion of soil pH during the dry and wet seasons in the Yinbei region of Ningxia, China, based on multi-source remote sensing data[J]. Geoderma Regional, 2021, 25: e00399.

[11] Bannari A, El-Battay A, Bannari R, et al. Sentinel-MSI VNIR and SWIR bands sensitivity analysis for soil salinity discrimination in an arid landscape[J]. Remote Sensing, 2018, 10(6): 855.

[12] Wang J, Ding J, Abulimiti A, et al. Quantitative estimation of soil salinity by means of different modeling methods and visible-near infrared (VIS–NIR) spectroscopy, Ebinur Lake Wetland, Northwest China[J]. PeerJ, 2018, 6: e4703.

[13] Jia Z, Tan Y, Guan X, et al. Saline-alkali soil formation and its remediation strategies in different regions of Ningxia: a comprehensive review[J]. J. Irrig. Drain, 2023, 42: 122-134.

[14] Tibin Z, Yaohu K, Wei H. Study on salinity characteristics of takyric solonetz in ningxia yinbei region[J]. Soil, 2012, 44(6): 1001-1008.

[15] Zhao W, Hu J, Li Z, et al. Variability and Modelling of Soil Moisture, Salt and Organic Matter Content in a Gravel-Sand Mulched Jujube Orchard[J]. Nature Environment & Pollution Technology, 2020, 19(4).